

Northumbria Research Link

Citation: Lasonder, Edwin, Green, Judith L., Grainger, Munira, Langsley, Gordon and Holder, Anthony A. (2015) Extensive differential protein phosphorylation as intraerythrocytic Plasmodium falciparum schizonts develop into extracellular invasive merozoites. *Proteomics*, 15 (15). pp. 2716-2729. ISSN 1615-9853

Published by: Wiley-Blackwell

URL: <https://doi.org/10.1002/pmic.201400508> <<https://doi.org/10.1002/pmic.201400508>>

This version was downloaded from Northumbria Research Link: <http://nrl.northumbria.ac.uk/42866/>

Northumbria University has developed Northumbria Research Link (NRL) to enable users to access the University's research output. Copyright © and moral rights for items on NRL are retained by the individual author(s) and/or other copyright owners. Single copies of full items can be reproduced, displayed or performed, and given to third parties in any format or medium for personal research or study, educational, or not-for-profit purposes without prior permission or charge, provided the authors, title and full bibliographic details are given, as well as a hyperlink and/or URL to the original metadata page. The content must not be changed in any way. Full items must not be sold commercially in any format or medium without formal permission of the copyright holder. The full policy is available online: <http://nrl.northumbria.ac.uk/policies.html>

This document may differ from the final, published version of the research and has been made available online in accordance with publisher policies. To read and/or cite from the published version of the research, please visit the publisher's website (a subscription may be required.)



Northumbria
University
NEWCASTLE

1 **Extensive differential protein phosphorylation as intraerythrocytic *Plasmodium***
2 ***falciparum* schizonts develop into extracellular invasive merozoites**

3

4

5 Edwin Lasonder^{1,*}, Judith L. Green², Munira Grainger², Gordon Langsley^{3,4,*}, Anthony A.
6 Holder^{2,*}

7

8

9

10 ¹School of Biomedical and Healthcare Sciences, A405 Portland Square, Plymouth
11 University, Drake Circus, Plymouth, Devon PL4 8AA, United Kingdom.

12 ²Division of Parasitology, MRC National Institute for Medical Research, The Ridgeway,
13 Mill Hill, London, NW7 1AA, United Kingdom.

14 ³Laboratoire de Biologie Cellulaire Comparative des Apicomplexes, Faculté de
15 Médecine, Université Paris Descartes - Sorbonne Paris Cité, France.

16 ⁴Inserm U1016, CNRS UMR8104, Institut Cochin, Paris, 75014 France.

17

18 *Corresponding authors

19

20 **Abstract**

21 Pathology of the most lethal form of malaria is caused by *Plasmodium falciparum*
22 asexual blood stages and initiated by merozoite invasion of erythrocytes. We present a
23 phosphoproteome analysis of extracellular merozoites revealing 1765 unique
24 phosphorylation sites including 785 sites not previously detected in schizonts. The
25 observed differential phosphorylation between extra and intraerythrocytic life cycle
26 stages was confirmed using both phospho-site and phospho-motif specific antibodies
27 and is consistent with the core motif [K/R]xx[pS/pT] being highly represented in
28 merozoite phosphoproteins. Comparative bioinformatic analyses highlighted protein
29 sets and pathways with established roles in invasion. Within the merozoite
30 phosphoprotein interaction network a sub-network of 119 proteins with potential roles in
31 cellular movement and invasion was identified and suggested that it is co-regulated by a
32 further small sub-network of protein kinase A (PKA), two calcium-dependent protein
33 kinases (CDPKs), a phosphatidyl inositol kinase (PI3K) and a GCN2-like eIF2-kinase
34 with a predicted role in translational arrest and associated changes in the ubiquitinome.
35 To test this notion experimentally, we examined the overall ubiquitination level in
36 intracellular schizonts versus extracellular merozoites and found it highly upregulated in
37 merozoites. We propose that alterations in the phosphoproteome and ubiquitinome
38 reflect a starvation-induced translational arrest as intracellular schizonts transform into
39 extracellular merozoites.

40

41

42 **1. Introduction**

43

44 The most lethal form of human malaria is caused by *Plasmodium falciparum*. This
45 parasite has a complex life cycle in both mosquito and human host, where asexual
46 multiplication and development within red blood cells (RBC) is responsible for disease
47 pathology. Intra-RBC parasite development is initiated by merozoite invasion of
48 erythrocytes, as merozoites are first released into the blood stream from merozoites in
49 the liver [1] and subsequently released at the end of each cycle of multiplication in RBC.
50 Preventing blood stage infection by targeting merozoites is an attractive intervention
51 strategy to develop treatments to alleviate disease. Therefore, understanding merozoite
52 development and the identification of new anti-malarial therapeutic targets are of the
53 utmost importance [2].

54 The merozoite is well adapted for RBC invasion [3]. It has the pellicular structure typical
55 of members of the Apicomplexa phylum including an apical end with secretory
56 organelles: micronemes, rhoptries and dense granules [4]. RBC invasion is a multi-step
57 process that is initiated by merozoite attachment, followed by reorientation and
58 sequential discharge of the contents of the apical organelles [5, 6]. During erythrocyte
59 entry, a process that is controlled in part by calcium and cAMP fluxes [7, 8], a moving
60 junction is formed between the parasite and host cell surfaces, and parasite proteins are
61 transferred to the newly invaded erythrocyte [8-10]. After invasion the parasite resides
62 within a parasitophorous vacuole and develops from a 'ring' to a trophozoite that
63 degrades host cell haemoglobin and performs DNA synthesis. The onset of mitosis
64 produces the multinucleated schizont, and following cell division individual merozoites

65 are formed, which are then released at the end of the cycle to infect new RBC [11].
66 Within erythrocytes the primary amino acid nutrient source for the developing parasite is
67 haemoglobin, which is degraded in the food vacuole. This structure is elaborated anew
68 following invasion [12] and haemoglobin digestion starts only several hours post-
69 invasion [13]. In late stage multinucleated “segmenter” schizonts that have undergone
70 cytokinesis, the food vacuole is 'pinched off' from the developing merozoites. Therefore,
71 merozoites and post-invasion early ring forms are deprived of haemoglobin-derived
72 amino acids for several hours. However, organelle degradation by autophagy likely
73 provides the developing merozoite and early ring stages with some nutrient [14].

74

75 Protein kinases, phosphatases and signal transduction pathways are integral to
76 regulation of the parasite life cycle; for example, both merozoite egress from the host
77 cell and erythrocyte invasion are governed by protein phosphorylation [15, 16].
78 Unravelling protein phosphorylation and signalling pathways in merozoites requires
79 large-scale phosphoproteome studies that are now feasible using mass spectrometry.
80 Significant efforts have been made in recent years to generate phosphoproteome data
81 principally for schizonts, leading to the identification of more than 12,000 unique protein
82 phosphorylation sites [17-22]. Our previous large scale phosphoproteome analysis of *P.*
83 *falciparum* schizonts by liquid chromatography tandem mass spectrometry (LC-MS/MS)
84 revealed extensive phosphatidylinositol and cAMP-dependent protein kinase (PKA)
85 signalling and identified three novel PKA substrates associated with the glideosome
86 motor complex that is implicated in driving the parasite into the RBC. These data
87 support a role for cAMP as an important regulator of host cell invasion [7, 18].

88 In this study we present a large-scale analysis of protein phosphorylation in extracellular
89 merozoites and its comparison with established schizont phosphoproteomes to deepen
90 our understanding of merozoite biology. We use bioinformatics to analyse
91 phosphorylation sites and establish a merozoite phosphoprotein interaction network.
92 Reassuringly this revealed a sub-network of merozoite proteins with predicted roles in
93 cellular movement and invasion. Interestingly, it also revealed a smaller sub-network of
94 five kinases known in other cellular systems to regulate starvation-induced translational
95 arrest and autophagy, both of which involve protein ubiquitination [23-26]. We confirm
96 global changes in phosphorylation patterns between schizonts and merozoites using
97 both commercial phospho-site specific antibodies and a specific phosphoprotein
98 antibody. Importantly, we show that differential phosphorylation is linked to highly
99 elevated ubiquitination in merozoites and we propose that alterations in the
100 phosphoproteome and ubiquitinome reflect starvation-induced translational arrest in
101 merozoites.

102

103

104 **2. Materials and Methods**

105

106 **2.1 Parasites.**

107 *P. falciparum* 3D7 line parasites were cultured *in vitro* as described previously [27].
108 Parasite populations were synchronised by treatment with sorbitol, Percoll gradient
109 centrifugation and passage through a magnetic column, allowing the purification of
110 merozoites as described [27, 28].

111

112 **2.2 In solution protease digestion and peptide purification using the Filter**
113 **Assisted Sample Preparation (FASP) method.**

114 Approximately $2-3 \times 10^9$ merozoites were lysed in 1 ml 2 % SDS in 50 mM Tris-HCl pH
115 7.3 in the presence of phosphatase and protease inhibitors. Halt™ phosphatase
116 inhibitor cocktail (Thermo Fisher) and complete protease inhibitor cocktail (Roche) were
117 used to suppress phosphatase and protease enzymatic activities. The Halt™
118 phosphatase cocktail is a concentrated solution of sodium fluoride, sodium
119 orthovanadate, sodium pyrophosphate and β -glycerophosphate, and was diluted 100-
120 fold for the final concentration. The complete protease inhibitor cocktail tablet contains
121 AEBSF, aprotinin, bestatin, E-64, leupeptin, pepstatin A and EDTA, and was diluted
122 according to the specifications of the manufacturer. The merozoite lysate was heated to
123 95°C for 5 min and further processed according to the FASP protocol [29]. The lysate
124 was divided and transferred to 12 0.5 ml Amicon Ultra 30K spin filter units (30 kDa cut-
125 off, Millipore), each of which was washed with 0.4 ml 8 M urea in 100 mM Tris-HCl pH
126 8.0 resulting in a final composition of 0.34% SDS and 5.8 M urea, then reduced with 10

127 mM DTT at room temperature (RT) for 25 min, concentrated by centrifugation at 14,000
128 g and alkylated in the dark with 50 mM iodoacetamide in 100 mM Tris-HCl pH 8.0
129 containing 8 M urea at RT for 25 min. The samples were concentrated by centrifugation
130 and diluted 10-fold with 100 mM Tris-HCl, 8 M urea, pH 8.0. This step was repeated 6
131 times to fully remove SDS from the lysate solution. Then, 2.5 µg lysC protease (Wako)
132 per sample was added in 100 mM Tris-HCl, 4 M urea, pH 8.0, and incubated overnight
133 at room temperature. Samples were further diluted with 50 mM ammonium bicarbonate
134 to a final concentration of 2 M urea and then incubated with 5 µg trypsin (Promega) for
135 18 h. The tryptic digest was acidified in 0.1 % (vol/vol) trifluoroacetic acid (TFA) and the
136 peptides purified and desalted with C18 Hypersil 500 mg SPE columns (Thermo
137 Fisher). Resultant peptides were separated by strong anion exchange (SAX) membrane
138 filters into six fractions on the basis of their isoelectric points. Peptides were eluted
139 stepwise with Britton and Robinson buffer solutions of decreasing pH: 8.0, 6.0, 5.0, and
140 4.0, respectively, followed by a final elution with 1 % TFA. All peptide fractions were
141 acidified immediately with 0.1 % TFA and then the peptides were purified again using
142 C18 Hypersil 500 mg SPE columns.

143

144 **2.3 Phosphopeptide enrichment.**

145 Peptides obtained from $2-3 \times 10^9$ purified merozoites, corresponding to 3 mg protein as
146 determined by a micro BCA protein assay kit (Thermo Fisher) were incubated with
147 Titansphere 10 µm TiO₂ beads (GL Sciences, Inc., Japan) to selectively purify
148 phosphorylated peptides, as described for the schizont phosphoproteome analysis [18].
149 Prior to incubation the TiO₂ beads were washed with 80% (vol/vol) acetonitrile, 0.1%

150 TFA, re-suspended in 30 mg/ml dihydroxybenzoic acid in 80% acetonitrile, 0.1% TFA
151 and diluted 1:4 with 0.1% TFA. Twenty microlitres of the slurry containing about 1 mg
152 beads were added to peptide solutions in 1.5 ml tubes and incubated under continuous
153 shaking for 1-2 h. Afterwards, the bead slurry was transferred to a micro spin column
154 made from a 200 µl precision pipette tip with an inserted 2mm fused silica frit (50 µm
155 internal diameter). Unbound fractions were collected following centrifugation of the spin
156 column and reincubated with freshly prepared TiO₂ bead slurry for 1-2 h. This step was
157 performed three times leading to four micro spin columns with TiO₂ beads per peptide
158 SAX fraction. The columns were washed three times by centrifugation with 100 µl 30%
159 acetonitrile, 3% TFA, followed by three washes with 100 µl 80% acetonitrile, 0.3% TFA.
160 Bound phosphopeptides were eluted from the beads with 100 µl 5 % NH₄OH, 5 %
161 piperidine, and 5 % pyrrolidine [30]. Peptide solutions were then acidified with TFA and
162 the peptides purified with STAGE tips [31] and dissolved in 0.1% TFA and 10 mM
163 EDTA.

164

165 **2.4 Liquid chromatography tandem mass spectrometry (LC-MS/MS).**

166 Tandem mass spectrometry experiments were performed with the linear ion trap
167 cyclotron resonance Fourier transform (LTQ-Ultra FT) mass spectrometer (Thermo
168 Fisher, Bremen, Germany) coupled to the nano EASY LC system (Proxeon, Denmark)
169 with 15 cm 100 µm internal diameter PicoTip columns (New Objective, Woburn, USA)
170 packed with 3 µm Reprosil C18 beads (Dr. Maisch GmbH, Ammerbuch, Germany).
171 Peptides were separated by liquid chromatography using a gradient from 92% buffer A
172 /8% buffer B to 73% buffer A /27% buffer B (where buffer A is 0.5% acetic acid in water

173 and buffer B is 0.5% acetic acid in acetonitrile) with a flow-rate of 300 nl/min over 90
174 min. A voltage of 2.2 kV was applied for electrospray ionisation. Data-dependent
175 acquisition was performed for switching automatically between MS, MS2 and
176 phosphoric acid neutral loss triggered MS3 scan modes. Full-scan MS spectra of intact
177 peptides (m/z 350–1500) with an automated gain control accumulation target value of
178 1,000,000 ions were acquired in the Fourier transform ion cyclotron resonance cell
179 with a resolution of 50,000. The four most abundant ions were sequentially isolated and
180 fragmented in the linear ion trap by applying collision induced dissociation using an
181 accumulation target value of 10,000, a capillary temperature of 100°C, and a normalized
182 collision energy of 27%. Multi-stage activation was switched on for neutral loss
183 dependent MS3 fragmentation on the masses of phosphoric acid at charge states 2+,
184 3+ and 4+. The four most abundant ions were sequentially fragmented under identical
185 settings as for MSMS mode with a normalized collision energy of 40 %. A dynamic
186 exclusion of ions previously sequenced within 180 s was applied. All unassigned charge
187 states and singly charged ions were excluded from fragmentation. Sequencing
188 thresholds were set at 500 counts for MS2 and 5 counts for MS3. The mass
189 spectrometry data have been submitted to the ProteomeXchange Consortium
190 (<http://proteomecentral.proteomexchange.org>).

191

192

193 **2.5 Mascot Peptide identification and MaxQuant validation.**

194 Tandem mass spectrometry data were processed using the same procedure we applied
195 previously to the schizont phosphoproteome [18]. Briefly, Mascot generic peak lists
196 were generated by MaxQuant version 1.013.13 (<http://maxquant.org/>) [32] and
197 submitted to Mascot version 2.2 (Matrix Science) to search the *P. falciparum* database
198 downloaded from <http://plasmodb.org/plasmo/> and supplemented with the human
199 International Protein Index (IPI) database (<http://www.ebi.ac.uk/IPI>) and frequently
200 observed contaminants and concatenated with reversed copies of all entries. The
201 following search parameters were applied: peptide mass 10 ppm, MSMS mass
202 accuracy of 0.5 Da; enzyme cleavage: trypsin allowing 2 miscleavage sites; fixed
203 modification for cysteines by carboxyamidomethylation and variable modifications to
204 enable detection of phosphorylation at serine, threonine and tyrosine; oxidation of
205 methionine; deamidation of glutamine and asparagine and protein N-terminal
206 acetylation. Mascot search results were processed further by MaxQuant [32], where
207 peptides were filtered; requiring a minimal Mascot peptide score of 20 in combination
208 with the probability that the identification is wrong, the posterior error probability (PEP)
209 of 0.025, a minimal charge state of 2 and no more than two variable modifications per
210 peptide. Peptides and proteins with a false discovery rate (FDR) better than 1 % were
211 accepted. The phosphorylation site localization probability >0.75 was applied to obtain
212 phosphopeptide FDR of 1 % [33].

213

214

215 **2.6 Gene ontology analysis.**

216 All *P. falciparum* gene ontology analyses were performed with the software package
217 Ontologizer [34] (<http://compbio.charite.de/index.php/ontologizer2.html>), with the
218 following Open Biological Ontology and Gene association components from
219 <http://www.geneontology.org>: gene ontology v1.2.obo, goslim_generic.obo and
220 Gene_association.GeneDB-Pfalciparum_2011-5-31. The OPI GO terms were taken
221 from and rearranged to a gene association compatible file. Ontologizer was used to
222 identify overrepresented GO terms for the phosphoproteome relative to the background
223 of the *P. falciparum* proteome (~5500 proteins). GO term enrichment was computed by
224 the parent-child union approach and corrected for multiple testing by the Benjamini and
225 Hochberg method, and was considered significant for adjusted p-values lower than 0.05
226 [34].

227

228 **2.7 Motif analysis.**

229 Phosphorylation sites were categorized by their chemical properties as acidic, basic,
230 proline-directed, tyrosine or other by a decision tree method from [18, 35] as follows: 1/
231 Get the 6 neighbouring amino acids before and after the phosphorylation site. 2/ pY at
232 position 0 then classify as "Tyrosine." 3/ P at +1 then classify as "Proline-directed." 4/
233 positions +1 to +6 contain more than one D and E residues then classify as "Acidic." 5/
234 K or R at position -3 then classify as "Basic." 6/ D or E at +1, +2, or +3 then classify as
235 "Acidic." 7/ between -6 and -1 more than 2 K or R residues then classify as "Basic." 8/
236 remaining peptides classify as "Other".

237 Merozoite phosphorylation motifs were identified using MotifX [36] that tested for motif
238 overrepresentation in phosphorylated peptides with the following parameters:
239 phosphorylation motif window = 13 amino acids, P-value threshold = 1×10^{-4} for S and T
240 residues, 1×10^{-3} for Y residues, motif fold increase ≥ 2 , a motif frequency > 5 , and a
241 background of all *P. falciparum* proteins. MotifX analysis was performed for a normal
242 and a degenerate amino acid set. The degenerate amino acid set was enabled for
243 conservative amino acid substitutions within the motif window according to: A=AG,
244 D=DE, F=FY, K=KR, I=ILVM, Q=QN, S=ST, C=C, H=H, P=P, W=W. When different
245 motifs were found for a peptide by the analyses with different amino acid residues,
246 priority was given to the motif with the highest MotifX score. Sequence logos were
247 generated with Weblogo 3 at <http://weblogo.threeplusone.com/create.cgi>. The motifs
248 were matched to known protein kinase target motifs using CompariMotif [37] at
249 http://bioware.ucd.ie/~compass/biowareweb/Server_pages/comparimotif.php, and
250 matches with the highest scores were considered as potential links between
251 phosphorylation motifs and protein kinases.

252

253 **2.8 Phosphorylated protein interaction network analysis.**

254 The merozoite phosphoproteome interaction network was constructed from all *P.*
255 *falciparum* protein-protein interaction data with a minimum confidence level of 0.15
256 downloaded from the STRING database version 9.0 [38] that were matched with the
257 phosphorylated *P. falciparum* proteins identified in this study and visualized in
258 Cytoscape version 2.8.3 [39]. The merozoite phospho-interactome was analyzed for

259 highly connected nodes with the molecular complex detection (MCODE) clustering
260 algorithm [40] that was available as a Cytoscape plug-in using default parameters.

261

262 **2.9 Phospho-site, Phospho-motif and Protein Ubiquitin Western blots**

263 Antibodies to the peptide PQRKPL*SIEESF based on the sequence of amino acid
264 residues 41 to 52 of myosin tail domain interacting protein (MTIP) and containing a
265 phosphoserine corresponding to Ser47 [41] were prepared in a sheep and purified by
266 affinity chromatography on the phosphopeptide coupled to a solid support (University of
267 Dundee). Late schizonts and merozoites were purified using a magnet and lysed in 30
268 cell-pellet volumes of NP40 lysis buffer (0.5% Nonidet P40, 150 mM NaCl, 50 mM Tris-
269 HCl pH 8.0) containing protease inhibitors (Roche). Following incubation on ice for 20
270 min, the soluble protein solution was collected after centrifugation at 15,000 g for 20 min
271 at 4°C. The merozoite lysate was either untreated or treated with Lambda phosphatase
272 (New England Biolabs), using five units phosphatase/μg protein and incubation for 20
273 min at 30°C, then the enzyme was heat inactivated at 65°C for 10 min. Lysates
274 containing approximately 10 μg protein were resolved on 10% NuPAGE Bis-Tris gels in
275 MOPS buffer (Life Technologies) under reducing conditions and the proteins transferred
276 to nitrocellulose using an iBlot system (Life Technologies). The blot was blocked
277 overnight in phosphate buffered saline containing 1% (wt/vol) BSA and 0.2% (vol/vol)
278 Tween-20 (PBST). For western blotting the sheep anti-phosphopeptide antibodies (1
279 μg/ml) were pre-incubated with 10 μg/ml non-phosphorylated peptide for 1 h at room
280 temperature to deplete antibodies not specific for the phosphoserine and then incubated
281 with the blot. MTIP was also detected with a rabbit anti-MTIP specific antibody that has

282 been described previously [5]. All antibody dilutions were made in PBST; washes were
283 with the same buffer. After extensive washing, the appropriate horseradish peroxidase
284 (HRP)-conjugated anti-IgG secondary antibodies (Sigma) were used to detect bound
285 antibody using enhanced chemiluminescence (GE Healthcare) and fluorography.

286 Antibodies recognizing phospho-PKA (motif 3), phospho-PKB/Akt (motif 4), phospho-
287 PKD (motif 11) and phospho-tyrosine motifs were obtained from Cell Signaling
288 Technologies. Schizont and merozoite cell pellets were resuspended in isotonic 0.15%
289 saponin to lyse red blood cell membranes. Parasites were pelleted by centrifugation at
290 2400 *g* and then schizonts were resuspended in 10 volumes and merozoites in 50
291 volumes of lysis buffer (0.5% NP40, 150 mM NaCl, 0.5 mM EDTA, 10 mM Tris HCl pH
292 8.0). Protein concentrations were determined using a detergent-compatible protein
293 assay (DC-protein assay, Biorad), and 10 μ g of each sample were resolved on 10%
294 polyacrylamide gels as described above. Following protein transfer to nitrocellulose and
295 blocking overnight, antibodies diluted 1:1000 were added and incubated with the blot for
296 1 h at room temperature. Bound antibodies were detected with HRP-linked species-
297 specific secondary antibodies (Biorad) at a dilution of 1:5000, as described above.

298 To analyse ubiquitination in parasites, a time course of late stage schizonts was
299 prepared. Briefly, parasites were synchronized to a 1 h window and harvested at
300 appropriate time points during the cycle. After initial lysis of the RBC membrane using
301 0.15% saponin followed by centrifugation of the sample at 2400 *g*, parasites were lysed
302 in a buffer containing 4% CHAPS, 1% DTT, 6 M urea, and 2 M thiourea. Samples were
303 subjected to three freeze-thaw cycles, and then centrifuged at 100,000 *g*. The
304 concentration of protein in the supernatant was determined using the Biorad Protein

305 Assay, and 2 µg samples of each protein fraction were resolved on a 12% NuPAGE
306 Bis-Tris gel in MOPS buffer. Following transfer to nitrocellulose and blocking as
307 described above, an anti mono- and polyubiquitinated conjugate monoclonal antibody
308 directly conjugated to HRP (FK2H, Enzo Life Sciences) was used at 1000-fold dilution
309 and detected using ECL. CDPK1 was detected using a specific rabbit polyclonal
310 antibody as described previously [41].

311

312 **3. Results**

313

314 **3.1 The phosphoproteome of *P. falciparum* merozoites**

315 Free merozoites were purified after release from highly synchronous populations of
316 schizonts [27, 28], and processed for mass spectrometric phosphoproteome analysis by
317 the gel-free protein digestion procedure, Filter Assisted Sample Preparation (FASP).
318 Merozoites were solubilised in 0.34 % SDS/ 5.8M urea and the proteins digested with
319 the proteolytic enzymes lysC and trypsin. Phosphopeptides were affinity-purified using
320 TiO₂ beads, and then subjected to liquid chromatography-tandem mass spectrometry
321 (LC-MS/MS) measurements. Peptides were identified by Mascot searches [42] of
322 MS/MS spectra against protein databases comprising all *P. falciparum* and human
323 proteins. Preliminary peptide identifications were validated in reverse database
324 searches using MaxQuant [32], resulting in identification of 1765 *P. falciparum*
325 phosphopeptides with phosphorylation site localization [33] probabilities >0.75 and
326 representing 740 distinct proteins (Figure 1, Table S1). Peptide identification criteria
327 were: a Mascot score greater than 20, posterior error probability (PEP) less than 0.025,

328 and a phosphopeptide False Discovery Rate (FDR) less than 0.01. A small number of
329 phosphorylated human proteins were identified by these validation criteria: 24 proteins,
330 comprising 36 sites (data not shown). Almost all detected merozoite phosphopeptides
331 were mono-phosphorylated (99.6%), which is likely explained in part by the observed
332 bias in enrichment by TiO₂ beads for such peptides [43]. The phospho-amino acid
333 distribution of 80% pSer and 19.6% pThr resembled that of our previous analysis of
334 schizonts using similar methodology [18], with 84.4% and 13.2%, respectively. Tyrosine
335 phosphorylation was less frequent in merozoites (0.4 % of phospho-sites) than in
336 schizonts (2.4 %). The observed low frequency of tyrosine phosphorylation in
337 merozoites highlights our stringent validation criteria since *Plasmodium* parasites lack
338 tyrosine kinases. *Plasmodium* proteins are probably phosphorylated by human tyrosine
339 kinases, and we speculate that host tyrosine kinase activity on extracellular merozoites
340 is likely lower than during intracellular schizont development, where we found a
341 frequency of 2.4 %. A comparative analysis of our merozoite data with the combined
342 data representing 12,252 phosphorylation sites derived from schizonts [18-22] revealed
343 a similar distribution in this combined set, with frequencies of 81.8 % (pSer), 14.4 %
344 (pThr), and 3.8% (pTyr), respectively (Figure 1). The merozoite phosphoproteome
345 contained 785 phosphorylated sites (Figure 1) that were not found among the 12,252
346 phosphorylation sites reported for schizonts. Several sites in merozoite proteins
347 implicated in erythrocyte invasion were found to be phosphorylated in both schizonts
348 and merozoites such as S610 of AMA1, and others such as S1240 of Sub2 appear to
349 be specifically phosphorylated in schizonts. However phosphorylation at some sites in
350 such proteins, for example residues 1024, 1246 and 1261 in MSP1; 1299 in EBA181;

351 and 137, 139, and 296 in RAP1, appears to be specific to the merozoite fraction (Table
352 S1); the functional significance of this is unknown. The proteome data generated in this
353 study comes from a single biological experiment measuring purified merozoites and
354 contains phosphopeptides with not more than 1 % false identifications.

355

356 **3.2 Functional annotation of the merozoite phosphoproteome**

357 The potential relevance of the merozoite phosphoproteome to parasite invasion biology
358 was assessed by functional enrichment analyses of the 740 phosphorylated merozoite
359 proteins relative to the full *P. falciparum* proteome (~ 5500 proteins). Firstly, a
360 comparative GO enrichment analysis was performed on extra (merozoites)- versus
361 intra-erythrocytic (schizonts) life cycle stages to identify any GO terms that were
362 significantly altered for the merozoite phosphoproteome using an extended set of
363 putative Gene Ontology (GO) annotations obtained from Ontology-based Pattern
364 Identification (OPI) clustering [44]. GO terms enriched in the merozoite
365 phosphoproteome (this study) were compared with enriched terms in the ensemble of
366 schizont phosphoproteomes represented by 12,252 phosphorylation sites detected
367 previously [18-22]. Statistical relevance in GO term enrichment between merozoites and
368 schizonts was assessed by Fisher exact tests (Table S2). The GO terms more than two-
369 fold enriched in the merozoite- relative to schizont-phosphoproteomes are shown in
370 Figure 2. We note that the enriched GO terms 'protein secretion', 'secretion', and
371 'secretion by cell' were not found to be statistically relevant, and neither are GO terms
372 represented by less than five proteins in the merozoite phosphoproteome (e.g. 'ATPase

373 activity, coupled to transmembrane movement of ions' and 'rhoptry'), even though the
374 differences appear striking.

375 In the category 'Molecular Function' (red columns, Figure 2 and see Table S3) we found
376 differences between merozoites and schizonts for terms associated with
377 phosphorylation such as 'lipid kinase activity' ($p < 0.05$) and 'calmodulin-dependent
378 protein kinase activities' ($p < 0.1$), as well for 'protein degradation', 'threonine-type
379 peptidase' and 'endopeptidase activities' ($p < 0.05$). GO terms in the category 'cellular
380 components' (green columns) were enriched ($p < 0.1$) in invasion-related components
381 such as 'apical part of cell' and 'apical complex' and significantly enriched ($p < 0.05$) for
382 'ubiquitin-mediated degradation' and 'proteasome core complex'. Finally, 16 biological
383 process (blue columns) were identified as enhanced in the merozoite phosphoproteome
384 including 11 with statistical relevance ($p < 0.05$) and 1 with $p < 0.1$. These terms included
385 'cellular response to stress' and three terms related to 'movement and locomotion' that
386 were most enriched ($p < 0.05$) in the merozoite phosphoproteome.

387 A second functional enrichment analysis was carried out with manually curated
388 pathways from the Metabolic Malaria Pathway database (MMPD)
389 (<http://priweb.cc.huji.ac.il/malaria/>). Enrichment in the merozoite phosphoproteome was
390 compared with enrichment in the ensemble of schizont phosphoproteomes (Figure 3;
391 Table S3). More than two-fold difference in enrichment ($p < 0.05$) between merozoites
392 and schizonts was observed for 'histone acetylation', and 'phosphoinositides and
393 membrane traffic'. The first term suggests an epigenetic change in gene expression in
394 merozoites. We previously highlighted extensive phosphatidyl inositol signalling in
395 schizonts [18] and now with the identification of eleven phosphorylated proteins involved

396 in inositol phosphate metabolism the current analysis argues that phosphatidyl inositol
397 signalling is even more elevated in merozoites. This would likely strongly activate
398 phosphatidyl inositol 3-phosphate kinase (PI3K)/Vps34 [45]. Importantly, two terms
399 'Genes coding for components of the proteasome degradation machinery' and
400 'proteasome-mediated proteolysis of ubiquitinated proteins' were also significantly
401 enriched ($p < 0.05$).

402

403 **3.3 Protein interaction network of the merozoite phosphoproteome**

404 We demonstrated previously that specific phosphorylated protein complexes in *P.*
405 *falciparum* schizonts have the potential to regulate most of the biological activities at this
406 stage [18]. Therefore, the merozoite phosphoproteome was mapped onto predicted
407 protein-protein interactions from the STRING database [38] to construct a scale-free
408 protein-interaction network of phosphorylated merozoite proteins. STRING is a protein-
409 protein interaction database of known interactions (from high throughput experiments
410 and literature mining) and predicted interactions (from genomic context and co-
411 expression) currently covering approximately 1100 species including *P. falciparum*. The
412 constructed merozoite interactome is composed of 682 nodes/proteins covering 92% of
413 the phosphoproteome and 19,584 edges corresponding to protein-protein interactions.
414 The global interaction network was analysed for the presence of densely connected
415 sub-networks using the molecular complex detection (MCODE) clustering algorithm
416 [40]. This allowed the identification of 20 sub-networks (Table S4), with the majority
417 interconnected via the hub of 4 proteins present in MCODE 13 (Figure 4A). Putative
418 biological functions of the different MCODE clusters were assigned by MMPD

419 enrichment analyses, as described above. This resulted in potential functional
420 annotations for 12 MCODE clusters representing 50% (369 proteins) of the merozoite
421 phosphoproteome (Figure 4B). Their assignments are in good agreement with the
422 MMPD enrichment analysis (Figure S1), and in some cases reinforced the proposed
423 biological functions. For example, MCODE cluster 16 comprised of 4 phosphorylated
424 proteins involved in inositol phosphate metabolism is 34-fold more enriched in the
425 cluster than in the full merozoite phosphoproteome (Figure 4B). Similarly, the hub
426 cluster MCODE 13 is 30-fold more enriched and is composed of three kinases
427 (PF3D7_1428500, a putative GCN2; PF3D7_0515300 [PI3K]; and PF3D7_0610600,
428 calcium dependent protein kinase 2 [CDPK2]), and the regulatory subunit
429 (PF3D7_1223100) of cAMP-dependent protein kinase [PKA]).

430

431 MCODE cluster 1 was identified as the largest sub-network composed of 119 phospho-
432 proteins with potentially 5739 protein-protein interactions (Figure 4A). It is under-
433 represented in schizont phosphorylation sites ($p < 0.05$) (Table S4), indicating an
434 enhanced role for this cluster in merozoite-related processes. Consistently, 23 proteins
435 had MMPD terms such as 'components of the linear motor responsible for merozoite
436 motility in invasion', 'domains of merozoite surface proteins', 'functional annotation of
437 merozoite invasion-related proteins', 'subcellular localization of proteins involved in
438 invasion' and 'genes coding for GPI-anchored membrane proteins'. Interestingly, four
439 proteins were associated with the ATG autophagic pathway (Figure 4B). Involvement of
440 proteins in the MCODE 1 cluster with cell invasion was further supported by enrichment
441 in GO annotations for 'locomotion and movement' (9.2-fold) covering 49 proteins of

442 which 13 were annotated to 'the apical complex' (12.0-fold), pointing again to a role in
443 invasion (Table S5). The functional significance for 'locomotion and movement' of this
444 sub-network was further supported by large differences in fold enrichment between
445 MCODE cluster 1 (9.2-fold) and the merozoite phosphoproteome (2.0-fold) showing that
446 these putative functions are concentrated in the sub-network. The detection of highly
447 enriched protein kinase activities for PKA (11.9-fold) and CDPK (9.3-fold) suggests a
448 regulatory role for these kinases in controlling MCODE cluster 1 activity. MCODE1
449 activities are likely co-regulated (depicted with yellow circles) by MCODE13 with for
450 example, PKAr of MCODE13 regulating PKAc catalytic activity in MCODE1 (see Fig.
451 S1). Similarly, the autophagy pathway may be co-regulated by MCODE 13 via direct
452 interaction of CDPK5 and PKAr with ATG8.

453 The presence in MCODE1 of PKG (PF3D7_1436600), GC α (PF3D7_1138400) and
454 PKAc (PF3D7_0934800), together with CDPK1 (PF3D7_0217500) and CDPK5
455 (PF3D7_1337800) indicates that in merozoites there is significant crosstalk between the
456 secondary messenger cyclic nucleotides and calcium [7, 8]. We have noted previously
457 that in schizonts both CDPK1 and GAP45 (PF3D7_1222700) could be phosphorylated
458 *in vitro* by PKA [18]. The presence of the putative zinc finger transcription factor KROX1
459 (PF3D7_1209300) in MCODE1 now suggests that this crosstalk could have a
460 transcriptional outcome, as cAMP and Ca²⁺ surges do on activating the transcription
461 factor Creb in mammalian cells [46, 47].

462

463

464 **3.4 Phosphorylation motif analysis.**

465 The merozoite phosphoproteome data set described here together with an ensemble of
466 the reported phosphoproteomes of schizonts [18-22] enabled us to compare schizont to
467 merozoite phosphorylation motifs. Firstly, we compared phosphorylation motif classes
468 based on their chemical properties using a decision tree previously applied to our
469 schizont phosphoproteome [18] (Figure 5). The motif classes 'basic-directed' and 'other'
470 are overrepresented in merozoites (fold-changes: 2.0 and 1.3, respectively) compared
471 to schizonts, while acidic-, proline- and tyrosine-directed classes are underrepresented
472 (fold-changes: -2.0, -1.5 and -7.3, respectively). Tyrosine phosphorylation is almost
473 absent in merozoites with only 9 sites found, suggesting that tyrosine kinase activity
474 may modify parasite proteins in schizonts, but not merozoites (see also Figure 6).

475 Secondly, phosphorylation sites identified in merozoites were classified using the
476 phosphorylation motif finding algorithm MotifX [36]. We identified 33 phosphorylation
477 motifs (Table S6) of which only five were reported in schizonts [18] [19, 21]. Within the
478 top 10 most abundant motifs we find 5 variants of the core motif [K/R]xx[S/T] covering
479 32.4 % of all phosphopeptides detected in merozoites. The 33 motifs contain no acidic
480 residues (Asp and Glu), in contrast to schizonts, where 14 motifs were rich in these
481 residues [18]. When the 33 motifs were mapped to known kinase target sites using
482 CompariMotif [37], several ambiguous matches were observed (Table S7). However,
483 the core motif ([K/R]xx[S/T]) exactly matched to known calcium/calmodulin-dependent
484 protein kinase II and PKA substrates, while imperfect matches were observed to other
485 AGC kinases such as PKC, PKD, PKG and Akt/PKB.

486 A clear trend emerged among the top 8 most enriched phosphorylation sites implicating
487 upregulated calcium/calmodulin-dependent protein kinase and PKA activities in
488 merozoites compared to schizonts (Figure 5B). Furthermore, we found that MCODE
489 cluster 1 was 1.4-fold ($p < 0.05$) enriched for sites with the [K/R]xx[S/T] core motif
490 relative to the full merozoite phosphoproteome (Table S4). No other MCODE cluster
491 was found to be statistically significantly enriched for either the core motif or merozoite
492 specific sites (Table S4), strengthening the notion that cluster 1 is enriched for
493 merozoite-specific functions.

494 **3.5 Differential phosphorylation between schizonts and merozoites at the site-**
495 **specific level.**

496 The above global phospho-motif view of differential phosphorylation between schizonts
497 and merozoites was confirmed at a specific phospho-site level by examining the
498 phosphorylation status of Ser47 in MTIP (PF3D7_1246400), which is phosphorylated by
499 CDPK1 [41]. Serine 47 (KPL*S₄₇) in MTIP occurs within the core motif (K/R)xx[*S/T)
500 that we have shown above is enriched in merozoites. The specific anti-phospho-S47
501 antibody recognised MTIP in merozoites, but not in schizonts and this recognition was
502 phosphatase sensitive, clearly identifying S47 of MTIP as being specifically
503 phosphorylated only in merozoites (Figure 6A).

504

505 **3.6 Experimental testing of phospho-motif enrichment analysis confirms**
506 **differential phosphorylation between schizonts and merozoites *in vivo***

507 The differential distribution of specific phosphorylation motifs between schizont (S) and
508 merozoite (M) proteins was also confirmed using a panel of commercial phospho-motif
509 specific antibodies (Figure 6B). Remarkable differences in phosphorylation patterns
510 between schizonts and merozoites were observed with antibodies specific for a typical
511 PKA substrate (motif 3: RRx[pS/pT]), a typical PKB/Akt substrate (motif 4: Rxx[pS/pT])
512 and a typical PKD substrate (motif 11: LxRxx[pS/pT]). Notably, the abundant core motif
513 [K/R]xx[pS/pT] identified by MotifX analysis (section 3.4) would be recognised by
514 antibodies to phospho-motifs 3, 4 and 11 (Figure 6B). So, three independent phospho-
515 motif specific antibodies show that the core motif (K/R)xx[S/T] is distributed differently
516 between schizont and merozoites proteins *in vivo*. Proteins containing phospho-tyrosine

517 were difficult to detect using a specific anti-phosphotyrosine antibody, consistent with
518 detection of only 9 sites in the merozoite phosphoproteome.

519

520 **3.7 Experimental testing of GO and MMPD enrichment analyses shows that**
521 **proteins are highly ubiquitinated in merozoites compared to schizonts**

522 Our various comparative bioinformatics analyses indicated that merozoites are enriched
523 in phosphoproteins involved in 'cellular response to stress', 'proteasome core complex',
524 'proteasome-mediated proteolysis' (Figure 2), and the 'autophagic pathway' (Figure 4B);
525 a collection of terms that suggested heightened ubiquitin-mediated protein degradation
526 might be taking place in merozoites. To test this prediction we probed protein extracts
527 prepared from schizonts (42- and 45-hours post-invasion) and free merozoites with an
528 antibody reactive with both mono- and poly-ubiquitinated proteins (Figure 6C). In
529 merozoites there was a very marked increase in the level of ubiquitination compared to
530 schizonts.

531

532

533 **4. Discussion**

534

535 The *P. falciparum* life cycle is complex with dynamic protein phosphorylation at different
536 stages. Following erythrocyte invasion the intracellular parasite develops through ring,
537 trophozoite and schizont stages prior to the release of extracellular merozoites that
538 invade new erythrocytes. Signal transduction pathways regulating development of the
539 intraerythrocytic parasite have been identified by large scale phosphorylation screens of
540 particular stages with a focus on schizonts [18-22]. In this study we have generated a
541 phosphoproteome of extracellular merozoites, and compared it with an ensemble of
542 schizont phosphoproteomes [18-22]. We used a subtractive approach to identify
543 differential protein phosphorylation in merozoites, and identified 785 sites
544 phosphorylated in merozoites and 980 phosphorylation sites shared between
545 merozoites and schizonts. The large number of phosphorylation sites detected in the
546 ensemble of schizont phosphoproteomes (12,252) compared to the 1785 sites detected
547 in merozoites indicates with a reasonable degree of certainty that the 785 sites
548 described in this study are merozoite specific.

549 At the phosphopeptide level we observed large differences in the distribution of specific
550 phosphorylation motifs, with 28 motifs not previously observed in schizonts. In addition,
551 the core motif sequence [K/R]xx[pS/pT] was highly enriched in merozoites being
552 contained in 35 % of the 28 phospho-motifs; a significant enrichment that directly
553 implicates upregulated calcium-dependent protein kinase and cAMP-dependent PKA
554 activities in the biology of merozoites. The overall differential distribution of
555 phosphorylated motifs was confirmed *in vivo* using commercial specific phospho-motif

556 antibodies to probe schizont and merozoite protein extracts. Three independent anti-
557 phospho-motif antibodies confirmed that schizonts and merozoites are differentially
558 phosphorylated. Consistently, the core motif [K/R]xx[pS/pT] that's enriched in
559 merozoites is common to all 3 phospho-motifs likely explaining some of the common
560 phospho-bands identified by western blot. This global view of differential
561 phosphorylation does not identify given phosphoproteins, so we examined S47 in MTIP,
562 as this residue occurs within the core motif imbedded in KPL*SIE. A specific phospho-
563 S47 antibody demonstrated that S47 in MTIP is clearly differentially phosphorylated
564 between schizonts (off) and merozoites (on). Thus, *in vivo* differential phosphorylation
565 occurs between schizonts and merozoites both at the site-specific and global levels.

566

567 We argue that differential phosphorylation translates into functional differences in
568 parasite biology that are highlighted by comparative gene ontology and pathway
569 enrichment analyses. In both cases we observed an increase in terms involved in
570 invasion biology (Figure 3, Table S2 and Table S3). This finding was corroborated by
571 cluster analysis of the merozoite phosphoprotein interaction network, where the largest
572 MCODE cluster (119 proteins) is also enriched for invasion biology. Besides invasion
573 biology we find the ATG autophagy pathway also enriched in MCODE1, and together
574 these observations lead us to propose that developing merozoites undergo starvation-
575 induced translational arrest, since they no longer have access to amino acids derived
576 from haemoglobin degradation. The marked increased in ubiquitination is consistent
577 with autophagic digestion of organelles no longer required by merozoites to invade.
578 Organelle and protein degradation would provide the necessary nutrient (lipid and

579 amino acids) for merozoites to survive the hostile extracellular environment, before they
580 elaborate a new food vacuole to digest host cell proteins such as haemoglobin [12, 13].
581 This upregulation of ubiquitination in extracellular merozoites compared to schizonts
582 has not been reported previously; in an earlier study ubiquitination was examined in
583 intracellular ring, trophozoite and schizont stages but merozoites were not included in
584 this analysis [48].

585

586

587 **Acknowledgements**

588 This work was supported by the FP7 projects MALSIG (HEALTH-F3-2009-223044 –
589 MALSIG) for EL, GL and AH and Network of Excellence EviMalaR (Health-2009-2.3.2-
590 1-242095) to EL and AH. The AH laboratory was supported by the MRC (File Reference
591 U117532067). Infrastructural support to the GL laboratory was provided by INSERM
592 and CNRS and GL also acknowledges support from the ParaFrap network of excellence
593 (ANR-11-LABX-0024). We gratefully acknowledge Hagai Ginsburg for providing MMPD
594 spreadsheets for pathway enrichment analysis. The antibodies specific for
595 phosphoSer47-MTIP were a kind gift from Dr Debbie Taylor. We thank the Nijmegen
596 Proteomics Facility for usage of the LC-MS instrumentation to carry out this study.

597

598 **FIGURE LEGENDS**

599

600 Figure 1: The merozoite phosphoproteome of *Plasmodium falciparum*.

601 A: Schematic overview of the phosphoproteome workflow. Steps in the workflow to
602 identify phosphopeptides in protease digests derived from $2-3 \times 10^9$ purified *P. falciparum*
603 merozoites. After lysis proteins were digested in solution with lysC and trypsin and
604 partially purified using FASP. Peptides were fractionated by strong anion exchange
605 (SAX) disks, enriched for phosphopeptides by TiO_2 and measured by liquid
606 chromatography tandem mass spectrometry. Phosphopeptides were identified by
607 Mascot database searches and validated by MaxQuant at 1 % FDR. A detailed
608 description of the procedure is provided in Experimental Procedures.

609 B: Venn diagram depicting overlap in protein phosphorylation sites between merozoite
610 and schizonts ensemble from previous studies [18-22].

611

612 Figure 2. GO annotation of the phosphoproteomes of asexual blood stages.

613 Comparative gene ontology enrichment analysis between the phosphoproteomes of
614 merozoites and schizont stages. Enrichment is shown for OPI-GO terms relative to all
615 5500 *P. falciparum* proteins. Statistical significance was tested using a one-tailed
616 Fisher exact test.

617

618

619 Figure 3. Pathway annotation of the phosphoproteomes of asexual blood stages.
620 Comparative pathway enrichment analysis between the phosphoproteomes of
621 merozoites and schizont life cycle stages. Enrichment is shown for increased MMPD
622 pathway terms relative to all 5500 *P. falciparum* proteins. Statistical significance was
623 tested using a one-tailed Fisher exact test (FET). We accepted pathways with p (FET)
624 < 0.005 in this figure. Pathways with lower significance ($0.005 < p < 0.05$) are provided
625 in Table S3.

626

627 Figure 4. The protein interaction network of the merozoite phosphoproteome.

628 A: Sub-networks of the phosphoprotein interaction network in merozoites. Protein
629 interaction data were downloaded from STRING and superimposed on the merozoite
630 phosphoproteome. Twenty sub-networks were identified by the MCODE clustering
631 algorithm. Here MCODE clusters are shown that interact with the central kinase cluster
632 MCODE 13.

633 B: MMPD pathway annotation of all MCODE clusters. A pathway enrichment analysis
634 was performed against the background of all 5500 proteins, and a clustering analysis
635 was performed to display functional divergence between MCODE clusters. Enriched
636 pathways in MCODE 1 are shown in yellow.

637

638

639 Figure 5: Protein phosphorylation motifs detected in merozoites.

640 A: Distribution of phosphorylation classes (acidic, basic, proline-directed, tyrosine and
641 other) in blood stages with merozoites in blue bars and schizonts in red bars.

642 B: Core phosphorylation motifs from the top 10 most abundant motifs in merozoites
643 represented by 13-mer sequence logos. Amino acids of the core motif sequence [K/R] x
644 x [S/T] are highlighted by red boxes.

645

646 Figure 6. Differential phosphorylation and ubiquitination of proteins in schizonts and
647 merozoites.

648 A: Western blot of schizont (S) and merozoite (M) protein extracts probed with an
649 antibody specific for phosphorylated Ser47 in MTIP. The antibody only reacted with
650 MTIP in merozoite extracts despite the presence of the protein in both schizonts and
651 merozoites. Treatment of the merozoite extract with phosphatase (+) abolished the
652 antibody reactivity confirming that phosphorylation of Ser47 was essential for antibody
653 recognition. The presence of MTIP in both schizont and merozoite extracts is displayed
654 with an antibody raised to recombinant MTIP.

655 B: Western blot of schizont (S) and merozoite (M) protein extracts probed with
656 phosphorylated phospho-motif-specific antibodies. The bands recognised by the
657 antibodies specific to motifs 3, 4 and 11 showed a differential pattern between schizonts
658 and merozoites, whereas the anti-phosphotyrosine antibody showed only weak
659 reactivity with both schizont and merozoite extracts. Anti-CDPK1 antibodies were used
660 as a loading control.

661 C: Western blot of schizont protein extracts made 42 and 45 h post-invasion together
662 with protein extracts made from free merozoites (M), probed with an antibody to mono-
663 and poly-ubiquitinated proteins. The strong reactivity with merozoite proteins indicates
664 an increased level of ubiquitination in merozoites compared to schizonts. Anti-CDPK1
665 antibodies were used as a loading control in the bottom panel.
666 The mobility of molecular mass markers (in kDa) is indicated on the left side of the
667 panels.
668

669 **Supplementary data**

670

671 **Table S1:** Phosphopeptide identification in the merozoite phosphoproteome.

672

673 **Table S2:** Gene Ontology enrichment results comparing the merozoite
674 phosphoproteome with the schizont phosphoproteome ensemble.

675

676 **Table S3:** MMPD pathway enrichment comparing the merozoite phosphoproteome with
677 the schizont phosphoproteome ensemble.

678

679 **Table S4:** List of MCODE proteins.

680

681 **Table S5:** GO enrichment results for MCODE cluster 1.

682

683 **Table S6:** Phosphorylation motifs detected in merozoites.

684

685 **Table S7:** Kinase substrates predicted by CompariMotif.

686

687 **Figure S1.** Protein- Protein Interactions between MCODE 1 and MCODE 13

688

689 **References**

690

- 691 [1] Sturm, A., Amino, R., van de Sand, C., Regen, T., *et al.*, Manipulation of host hepatocytes by
692 the malaria parasite for delivery into liver sinusoids. *Science* 2006, *313*, 1287-1290.
- 693 [2] Miller, L. H., Ackerman, H. C., Su, X. Z., Wellems, T. E., Malaria biology and disease
694 pathogenesis: insights for new treatments. *Nature medicine* 2013, *19*, 156-167.
- 695 [3] Bannister, L. H., Mitchell, G. H., Butcher, G. A., Dennis, E. D., Cohen, S., Structure and
696 development of the surface coat of erythrocytic merozoites of *Plasmodium knowlesi*. *Cell and*
697 *tissue research* 1986, *245*, 281-290.
- 698 [4] Cowman, A. F., Berry, D., Baum, J., The cellular and molecular basis for malaria parasite
699 invasion of the human red blood cell. *J Cell Biol* 2012, *198*, 961-971.
- 700 [5] Baum, J., Richard, D., Healer, J., Rug, M., *et al.*, A conserved molecular motor drives cell
701 invasion and gliding motility across malaria life cycle stages and other apicomplexan parasites. *J*
702 *Biol Chem* 2006, *281*, 5197-5208.
- 703 [6] Farrow, R. E., Green, J., Katsimitsoulia, Z., Taylor, W. R., *et al.*, The mechanism of
704 erythrocyte invasion by the malarial parasite, *Plasmodium falciparum*. *Seminars in cell &*
705 *developmental biology* 2011, *22*, 953-960.
- 706 [7] Dawn, A. S., S.; More, K.R.; Siddiqui, F.A.; Pachikara, N.; Ramdani, G.; Langsley, G.;
707 Chitnis, C.E., The Central Role of cAMP in Regulating *Plasmodium falciparum* Merozoite
708 Invasion of Human Erythrocytes. *PLoS Pathog* 2014, *10*, e1004520.
- 709 [8] Gao, X., Gunalan, K., Yap, S. S., Preiser, P. R., Triggers of key calcium signals during
710 erythrocyte invasion by *Plasmodium falciparum*. *Nat Commun* 2013, *4*, 2862.
- 711 [9] Billker, O., Lourido, S., Sibley, L. D., Calcium-dependent signaling and kinases in
712 apicomplexan parasites. *Cell Host Microbe* 2009, *5*, 612-622.
- 713 [10] Holder, A. A., Mohd Ridzuan, M. A., Green, J. L., Calcium dependent protein kinase 1 and
714 calcium fluxes in the malaria parasite. *Microbes and infection / Institut Pasteur* 2012, *14*, 825-
715 830.
- 716 [11] Gerald, N., Mahajan, B., Kumar, S., Mitosis in the human malaria parasite *Plasmodium*
717 *falciparum*. *Eukaryot Cell* 2011, *10*, 474-482.
- 718 [12] Dluzewski, A. R., Ling, I. T., Hopkins, J. M., Grainger, M., *et al.*, Formation of the food
719 vacuole in *Plasmodium falciparum*: a potential role for the 19 kDa fragment of merozoite surface
720 protein 1 (MSP1₁₉). *PLoS One* 2008, *3*, e3085.
- 721 [13] Abu Bakar, N., Klonis, N., Hanssen, E., Chan, C., Tilley, L., Digestive-vacuole genesis and
722 endocytic processes in the early intraerythrocytic stages of *Plasmodium falciparum*. *J Cell Sci*
723 2010, *123*, 441-450.
- 724 [14] Tomlins, A. M., Ben-Rached, F., Williams, R. A., Proto, W. R., *et al.*, *Plasmodium*
725 *falciparum* ATG8 implicated in both autophagy and apicoplast formation. *Autophagy* 2013, *9*,
726 1540-1552.
- 727 [15] Gaur, D., Chitnis, C. E., Molecular interactions and signaling mechanisms during
728 erythrocyte invasion by malaria parasites. *Current opinion in microbiology* 2011, *14*, 422-428.
- 729 [16] Jacot, D., Soldati-Favre, D., Does protein phosphorylation govern host cell entry and egress
730 by the Apicomplexa? *International journal of medical microbiology : IJMM* 2012, *302*, 195-202.
- 731 [17] Lasonder, E., Treeck, M., Alam, M., Tobin, A. B., Insights into the *Plasmodium falciparum*
732 schizont phospho-proteome. *Microbes and infection / Institut Pasteur* 2012, *14*, 811-819.

733 [18] Lasonder, E., Green, J. L., Camarda, G., Talabani, H., *et al.*, The Plasmodium falciparum
734 schizont phosphoproteome reveals extensive phosphatidylinositol and cAMP-protein kinase A
735 signaling. *J Proteome Res* 2012, *11*, 5323-5337.

736 [19] Pease, B. N., Huttlin, E. L., Jedrychowski, M. P., Talevich, E., *et al.*, Global analysis of
737 protein expression and phosphorylation of three stages of Plasmodium falciparum
738 intraerythrocytic development. *J Proteome Res* 2013, *12*, 4028-4045.

739 [20] Solyakov, L., Halbert, J., Alam, M. M., Semblat, J. P., *et al.*, Global kinomic and phospho-
740 proteomic analyses of the human malaria parasite Plasmodium falciparum. *Nat Commun* 2011, *2*,
741 565.

742 [21] Treeck, M., Sanders, J. L., Elias, J. E., Boothroyd, J. C., The phosphoproteomes of
743 Plasmodium falciparum and Toxoplasma gondii reveal unusual adaptations within and beyond
744 the parasites' boundaries. *Cell Host Microbe* 2011, *10*, 410-419.

745 [22] Collins, M. O., Wright, J. C., Jones, M., Rayner, J. C., Choudhary, J. S., Confident and
746 sensitive phosphoproteomics using combinations of collision induced dissociation and electron
747 transfer dissociation. *Journal of proteomics* 2014, *103*, 1-14.

748 [23] Wek, R. C., Jiang, H. Y., Anthony, T. G., Coping with stress: eIF2 kinases and translational
749 control. *Biochemical Society transactions* 2006, *34*, 7-11.

750 [24] Funderburk, S. F., Wang, Q. J., Yue, Z., The Beclin 1-VPS34 complex--at the crossroads of
751 autophagy and beyond. *Trends in cell biology* 2010, *20*, 355-362.

752 [25] Harr, M. W., Distelhorst, C. W., Apoptosis and autophagy: decoding calcium signals that
753 mediate life or death. *Cold Spring Harb Perspect Biol* 2010, *2*, a005579.

754 [26] Tudisca, V., Simpson, C., Castelli, L., Lui, J., *et al.*, PKA isoforms coordinate mRNA fate
755 during nutrient starvation. *J Cell Sci* 2012, *125*, 5221-5232.

756 [27] Taylor, H. M., Grainger, M., Holder, A. A., Variation in the expression of a Plasmodium
757 falciparum protein family implicated in erythrocyte invasion. *Infection and immunity* 2002, *70*,
758 5779-5789.

759 [28] Blackman, M. J., Purification of Plasmodium falciparum merozoites for analysis of the
760 processing of merozoite surface protein-1. *Methods in cell biology* 1994, *45*, 213-220.

761 [29] Wisniewski, J. R., Zougman, A., Nagaraj, N., Mann, M., Universal sample preparation
762 method for proteome analysis. *Nat Methods* 2009, *6*, 359-362.

763 [30] Kyono, Y., Sugiyama, N., Imami, K., Tomita, M., Ishihama, Y., Successive and selective
764 release of phosphorylated peptides captured by hydroxy acid-modified metal oxide
765 chromatography. *J Proteome Res* 2008, *7*, 4585-4593.

766 [31] Rappsilber, J., Ishihama, Y., Mann, M., Stop and go extraction tips for matrix-assisted laser
767 desorption/ionization, nanoelectrospray, and LC/MS sample pretreatment in proteomics. *Anal*
768 *Chem* 2003, *75*, 663-670.

769 [32] Cox, J., Mann, M., MaxQuant enables high peptide identification rates, individualized
770 p.p.b.-range mass accuracies and proteome-wide protein quantification. *Nat Biotechnol* 2008, *26*,
771 1367-1372.

772 [33] Olsen, J. V., Mann, M., Improved peptide identification in proteomics by two consecutive
773 stages of mass spectrometric fragmentation. *Proc Natl Acad Sci U S A* 2004, *101*, 13417-13422.

774 [34] Bauer, S., Grossmann, S., Vingron, M., Robinson, P. N., Ontologizer 2.0--a multifunctional
775 tool for GO term enrichment analysis and data exploration. *Bioinformatics* 2008, *24*, 1650-1651.

776 [35] Huttlin, E. L., Jedrychowski, M. P., Elias, J. E., Goswami, T., *et al.*, A tissue-specific atlas
777 of mouse protein phosphorylation and expression. *Cell* 2010, *143*, 1174-1189.

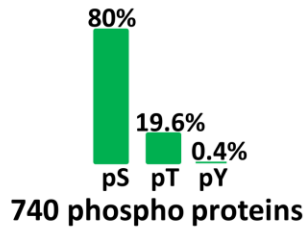
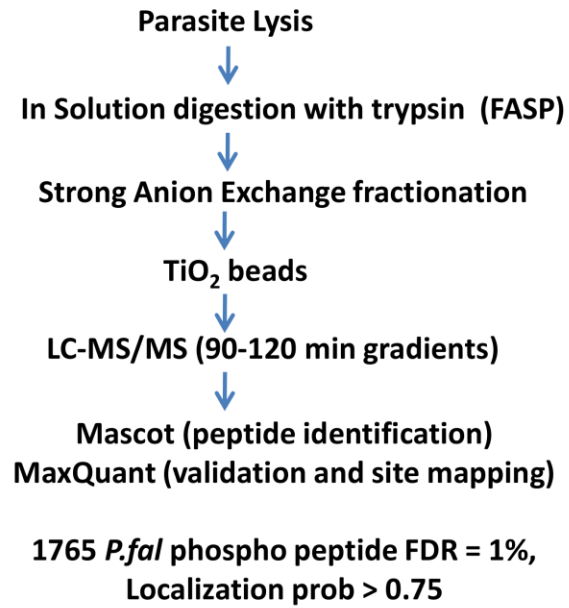
778 [36] Schwartz, D., Gygi, S. P., An iterative statistical approach to the identification of protein
779 phosphorylation motifs from large-scale data sets. *Nat Biotechnol* 2005, 23, 1391-1398.
780 [37] Edwards, R. J., Davey, N. E., Shields, D. C., CompariMotif: quick and easy comparisons of
781 sequence motifs. *Bioinformatics* 2008, 24, 1307-1309.
782 [38] Szklarczyk, D., Franceschini, A., Kuhn, M., Simonovic, M., *et al.*, The STRING database in
783 2011: functional interaction networks of proteins, globally integrated and scored. *Nucleic Acids*
784 *Res* 2011, 39, D561-568.
785 [39] Shannon, P., Markiel, A., Ozier, O., Baliga, N. S., *et al.*, Cytoscape: a software environment
786 for integrated models of biomolecular interaction networks. *Genome Res* 2003, 13, 2498-2504.
787 [40] Bader, G. D., Betel, D., Hogue, C. W., BIND: the Biomolecular Interaction Network
788 Database. *Nucleic Acids Res* 2003, 31, 248-250.
789 [41] Green, J. L., Rees-Channer, R. R., Howell, S. A., Martin, S. R., *et al.*, The motor complex of
790 *Plasmodium falciparum*: phosphorylation by a calcium-dependent protein kinase. *J Biol Chem*
791 2008, 283, 30980-30989.
792 [42] Perkins, D. N., Pappin, D. J., Creasy, D. M., Cottrell, J. S., Probability-based protein
793 identification by searching sequence databases using mass spectrometry data. *Electrophoresis*
794 1999, 20, 3551-3567.
795 [43] Thingholm, T. E., Jensen, O. N., Larsen, M. R., Enrichment and separation of mono- and
796 multiply phosphorylated peptides using sequential elution from IMAC prior to mass
797 spectrometric analysis. *Methods Mol Biol* 2009, 527, 67-78, xi.
798 [44] Zhou, Y., Ramachandran, V., Kumar, K. A., Westenberger, S., *et al.*, Evidence-based
799 annotation of the malaria parasite's genome using comparative expression profiling. *PLoS One*
800 2008, 3, e1570.
801 [45] Vaid, A., Ranjan, R., Smythe, W. A., Hoppe, H. C., Sharma, P., PfPI3K, a
802 phosphatidylinositol-3 kinase from *Plasmodium falciparum*, is exported to the host erythrocyte
803 and is involved in hemoglobin trafficking. *Blood* 2010, 115, 2500-2507.
804 [46] Poser, S., Storm, D. R., Role of Ca²⁺-stimulated adenylyl cyclases in LTP and memory
805 formation. *International journal of developmental neuroscience : the official journal of the*
806 *International Society for Developmental Neuroscience* 2001, 19, 387-394.
807 [47] Shaywitz, A. J., Greenberg, M. E., CREB: a stimulus-induced transcription factor activated
808 by a diverse array of extracellular signals. *Annu Rev Biochem* 1999, 68, 821-861.
809 [48] Ponts, N., Saraf, A., Chung, D. W., Harris, A., *et al.*, Unraveling the ubiquitome of the
810 human malaria parasite. *J Biol Chem* 2011, 286, 40320-40330.

811

812

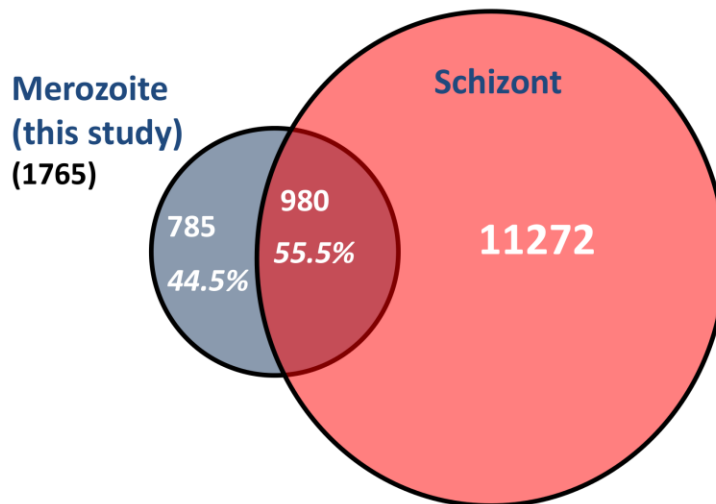
A

P. fal merozoites phospho-proteome workflow

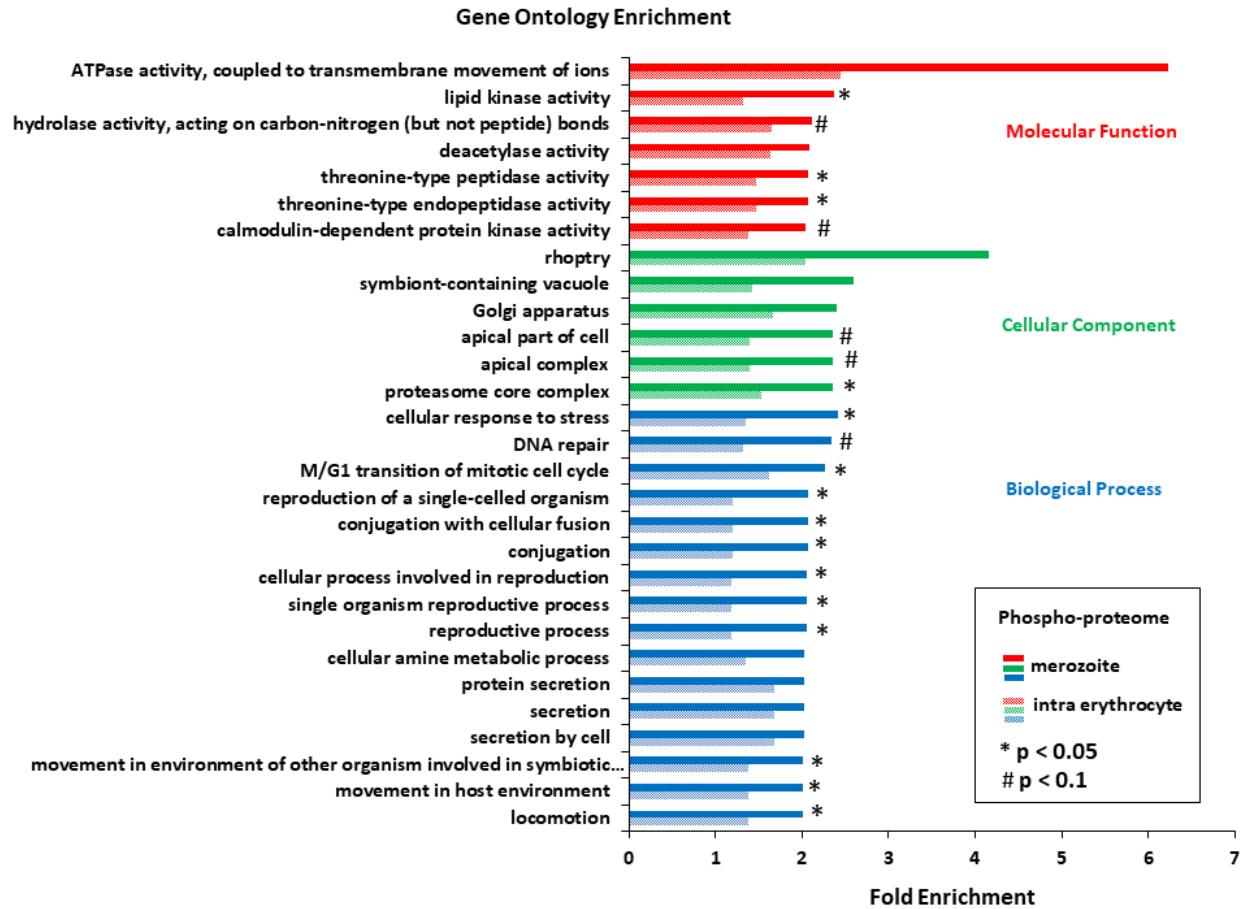


B

PHOSPHO PEPTIDE SITES



813
814 FIGURE 1



815

816

817 FIGURE 2

818

819

820

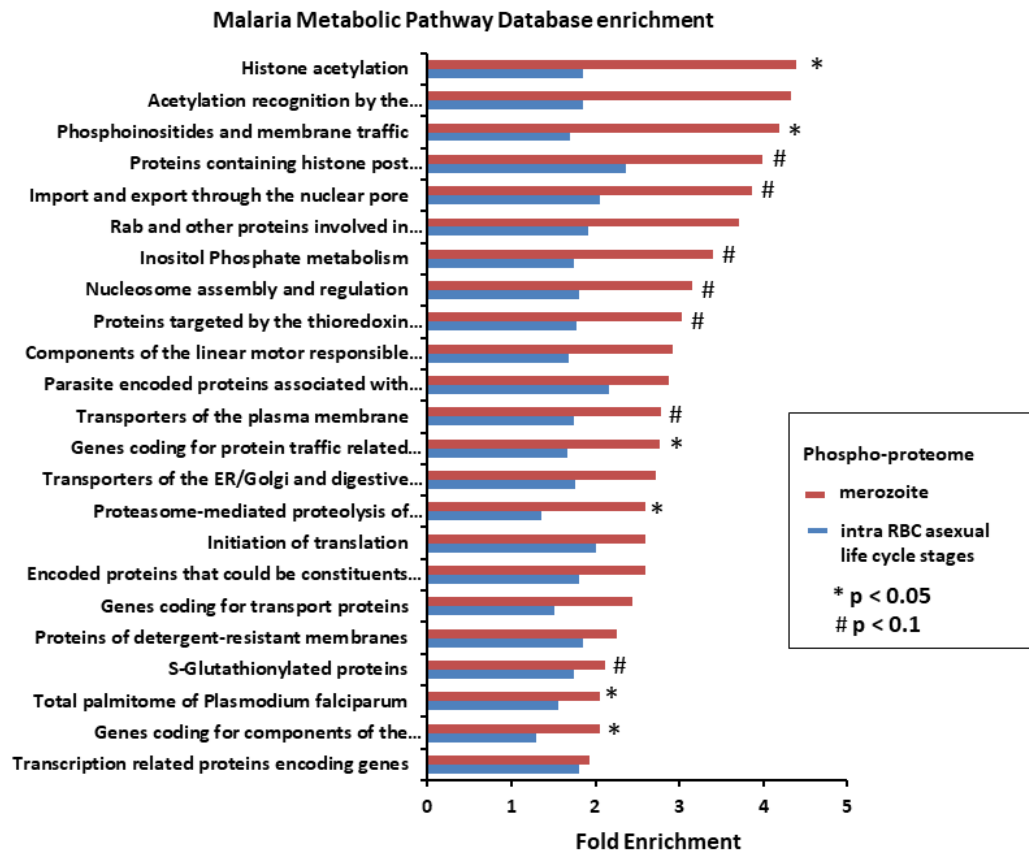
821

822

823

824

825



826

827 FIGURE 3

828

829

830

831

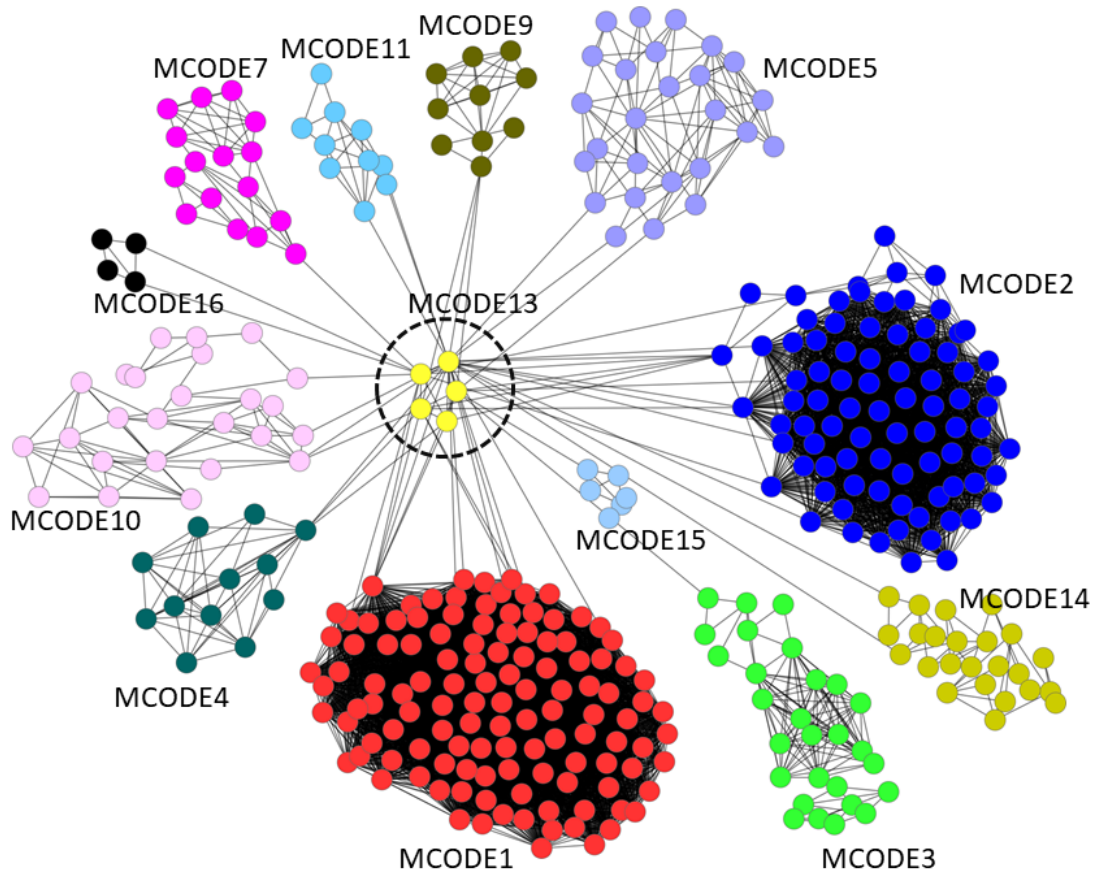
832

833

834

835

836



837

838

839 FIGURE 4A

840

841

842

843

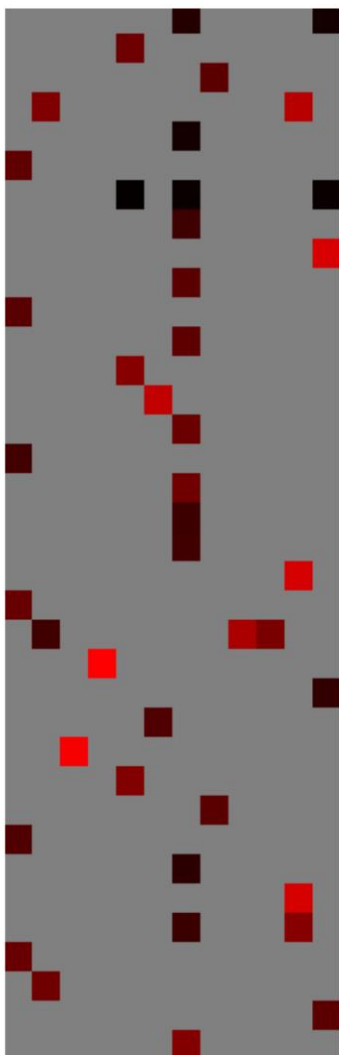
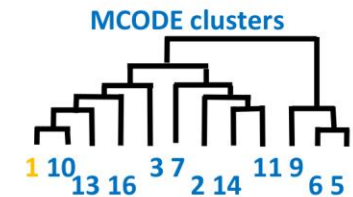
844

845

846

847

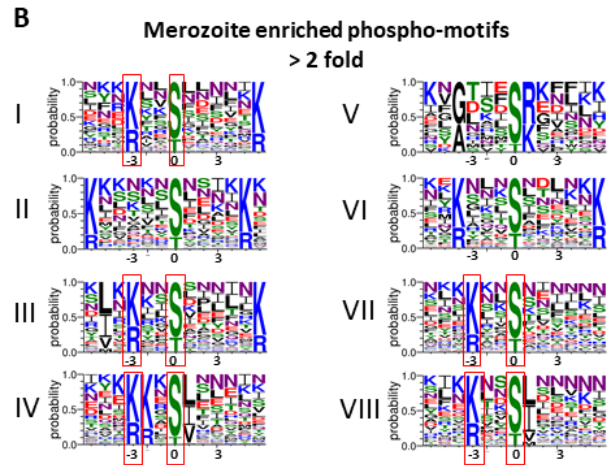
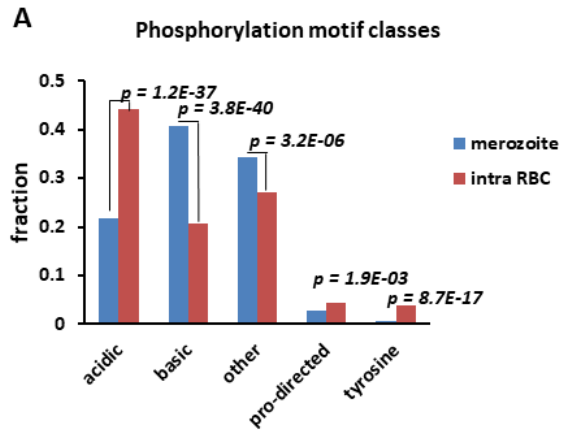
LOG2 FOLD ENRICHMENT



- S-Glutathionylated proteins
- The acidocalcisome
- Nucleosome assembly and regulation
- Genes involved in excision-repair
- Genes coding for chaperones and their regulators
- Functional annotation of merozoite invasion-related proteins
- Total palmitome of Plasmodium falciparum
- Maturation and export of 60S and 40S ribosomal subunits
- SRP-mediated targeting of membrane and secretory proteins
- Proteins targeted by the thioredoxin superfamily enzymes
- Subcellular localization of proteins involved in invasion
- Parasite encoded proteins associated with iRBC membrane
- Transporters of the plasma membrane
- Proteins containing histone PTM-binding modules
- Initiation of translation
- The ATG autophagic pathway
- Protein biosynthesis
- Proteome of the parasitophorous vacuole
- Chaperone-assisted protein folding
- DNA Replication
- Domains of merozoite surface proteins
- Genes coding for proteasome degradation machinery
- Inositol Phosphate metabolism
- Proteins of detergent-resistant membranes
- Transcription related proteins encoding genes
- Protein kinase coding genes
- Genes coding for transport proteins
- Established and putative Maurer's clefts proteins
- Compon. of linear motor resp. for meroz. motility in invasion
- Centrosome proteins
- Base excision repair of AP sites
- Genes coding for components involved in ribosome assembly
- Genes coding for GPI-anchored membrane proteins
- Nuclear genes with apicoplast signal sequences
- Splicing of pre-mRNA
- Ribosomal structure

848

849 FIGURE 4B



850

851 FIGURE 5

852

853

854

855

856

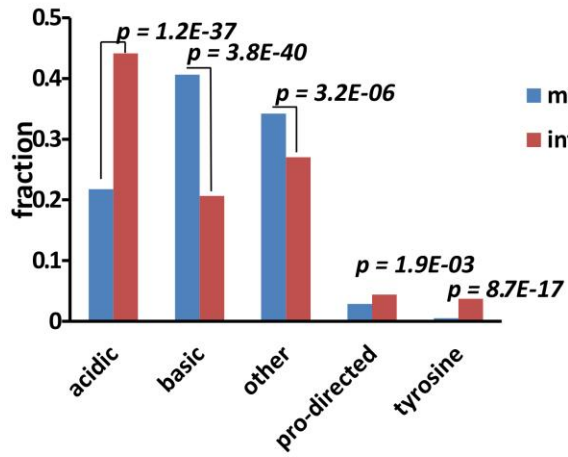
857

858

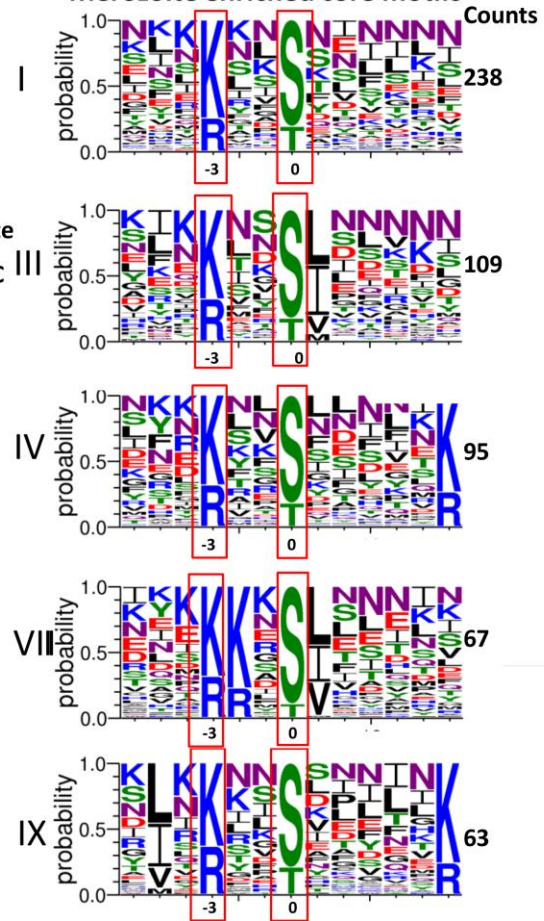
859

860

A Phosphorylation motif classes



B Merozoite enriched core motifs



861

862

863 FIGURE 6A

864

865

866

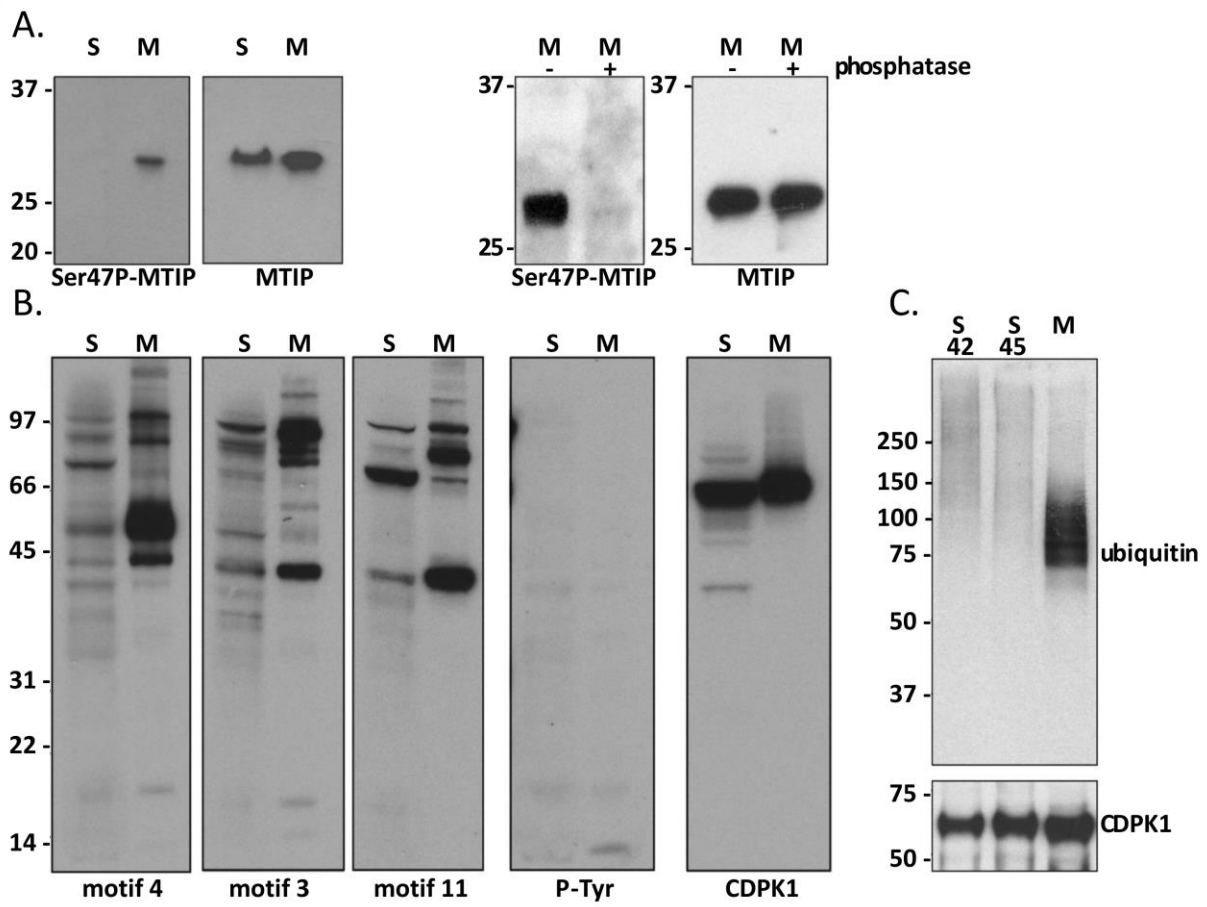
867

868

869

870

871



872

873

874 FIGURE 6B

875

876

877

878

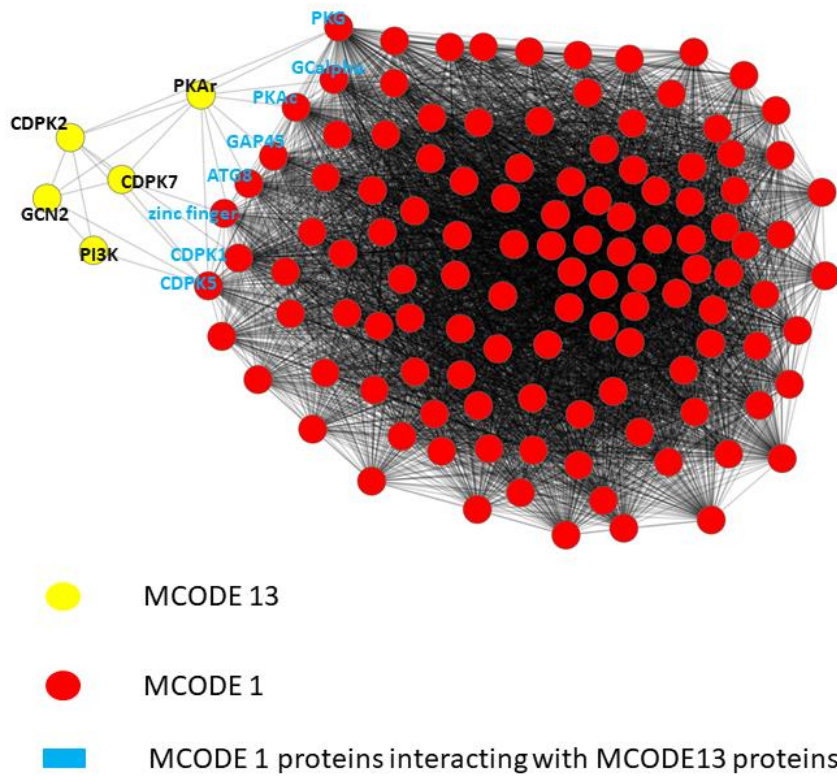
879

880

881

882

FIGURE S1. Protein- Protein Interactions between MCODE 1 and MCODE 13



883